Article:
Smith, L.J., Crowther, P.A., Calzetti, D. et al. (2016) The very massive star content of the nuclear star clusters in NGC 5253. ASTROPHYSICAL JOURNAL, 823 (1). ARTN 38. ISSN: 0004-637X

https://doi.org/10.3847/0004-637X/823/1/38

The Astrophysical Journal, 823:38 (10pp), 2016 May 20 doi:10.3847/0004-637X/823/1/38

THE VERY MASSIVE STAR CONTENT OF THE NUCLEAR STAR CLUSTERS IN NGC 5253

L. J. Smith[1], P. A. Crowther[2], D. Calzetti[3], and F. Sidoli[4]
[1] Space Telescope Science Institute and European Space Agency, 3700 San Martin Drive, Baltimore, MD 21218, USA; lsmith@stsci.edu
[2] Department of Physics and Astronomy, University of Sheffield, Sheffield S3 7RH, UK
[3] Department of Astronomy, University of Massachusetts—Amherst, Amherst, MA 01003, USA
[4] London Centre for Nanotechnology, University College London, London WC1E 6BT, UK
Received 2016 January 29; accepted 2016 March 22; published 2016 May 20

ABSTRACT

The blue compact dwarf galaxy NGC 5253 hosts a very young starburst containing twin nuclear star clusters, separated by a projected distance of 5 pc. One cluster (#5) coincides with the peak of the Hα emission and the other (#11) with a massive ultracompact H II region. A recent analysis of these clusters shows that they have a photometric age of 1 ± 1 Myr, in apparent contradiction with the age of 3–5 Myr inferred from the presence of Wolf-Rayet features in the cluster #5 spectrum. We examine *Hubble Space Telescope* ultraviolet and Very Large Telescope optical spectroscopy of #5 and show that the stellar features arise from very massive stars (VMSs), with masses greater than 100 $M_{\odot}$, at an age of 1–2 Myr. We further show that the very high ionizing flux from the nuclear clusters can only be explained if VMSs are present. We investigate the origin of the observed nitrogen enrichment in the circumcluster ionized gas and find that the excess N can be produced by massive rotating stars within the first 1 Myr. We find similarities between the NGC 5253 cluster spectrum and those of metal-poor, high-redshift galaxies. We discuss the presence of VMSs in young, star-forming galaxies at high redshift; these should be detected in rest-frame UV spectra to be obtained with the *James Webb Space Telescope*. We emphasize that population synthesis models with upper mass cutoffs greater than 100 $M_{\odot}$ are crucial for future studies of young massive star clusters at all redshifts.

Key words: galaxies: dwarf – galaxies: individual (NGC 5253) – galaxies: starburst – galaxies: star clusters: general – stars: massive – stars: Wolf–Rayet

1. INTRODUCTION

The blue compact dwarf galaxy NGC 5253 hosts a very young starburst at its center. The near absence of nonthermal radio emission (Beck et al. 1996) shows that the starburst is too young to have produced many supernovae. Wolf-Rayet (W-R) emission features from WN and WC stars were first detected by Campbell et al. (1986) and Schaerer et al. (1997) in groups of young star clusters, suggesting that the burst is 3–5 Myr old. The triggering process for the current starburst is not clear. An encounter with M83 has been suggested (van den Bergh 1980; Caldwell & Phillips 1989), or Cen A (Karachentsev et al. 2007; Tully et al. 2015). The distance to NGC 5253 is uncertain, with values of 3.1–4.0 Mpc quoted in the literature. Here we adopt a distance of 3.15 Mpc for NGC 5253 (Freedman et al. 2001; Davidge 2007) based on Cepheid and tip of the red giant branch (TRGB) measurements. We note that the most recent TRGB measurement places NGC 5253 at 3.55 Mpc (Tully et al. 2013). López-Sánchez et al. (2012) have performed an H I line and 20 cm radio continuum study of NGC 5253. They find that the H I morphology is very disturbed and suggest that the starburst is being triggered by the infall of a diffuse, low-metallicity H I cloud along the minor axis. The metallicity of NGC 5253 is fairly low, with the recent study of Monreal-Ibero et al. (2012) giving $12+\log \mathrm{O/H} = 8.26$, or 35% solar (using the solar oxygen abundance of Asplund et al. 2009). Recently, Turner et al. (2015) presented Submillimeter Array images of NGC 5253 showing evidence for a CO streamer falling into the center of the galaxy and possibly fueling the current star formation.

Turner et al. (1998) found that radio maps of the central region are dominated by a single unresolved source with the characteristics of a massive ultracompact H II region. Turner et al. (2000) resolved this source and found a bright, very dense radio nebula of dimensions $0\farcs10 \times 0\farcs04$ (1.5×0.6 pc) in the central starburst, which they term the "supernebula." The Lyman continuum rate required to excite the nebula is equivalent to a few thousand O7V stars within the central 2″ (Crowther et al. 1999; Turner & Beck 2004). *Hubble Space Telescope* (*HST*) observations with the Near Infrared Camera and Multi Object Spectrometer (NICMOS) by Alonso-Herrero et al. (2004) revealed the presence of a double nuclear star cluster with the two components separated by 0.″3–0.″4 (≈5 pc). The eastern cluster coincides with the peak of the Hα emission in NGC 5253 and is the youngest optical star cluster identified by Calzetti et al. (1997). The western cluster is very reddened and is coincident with the supernebula of Turner et al. (2000).

In a recent paper, Calzetti et al. (2015) present a detailed analysis of the two nuclear clusters (#5 and #11 in their terminology) using *HST* imaging from the far-ultraviolet to the infrared. By fitting their spectral energy distributions (SEDs), they find that the two clusters are extremely young, with ages of only 1 ± 1 Myr. The SED for cluster #5 can be fit with a foreground dust model, while a combination of a homogeneous dust–star mixture and a foreground dust screen is required for cluster #11. The derived cluster masses are 7.5×10^4 and 2.5×10^5 $M_{\odot}$ for #5 and #11, respectively. The predicted Hα luminosity for cluster #5 is higher than the observed, attentuation-corrected value, and this discrepancy is interpreted as being due to the leakage of 25%–50% of the ionizing photons into a larger ionized, diffuse region surrounding both clusters, and coincident with the radio nebula. For cluster #11, the predicted and observed attentuation-corrected Hα luminosities agree well and argue in favor of the SED fitting results. The young ages of the two nuclear star clusters are in apparent

contradiction with the ages of 3–5 Myr inferred from the presence of W-R stars in cluster #5 (e.g., Monreal-Ibero et al. 2010; Turner et al. 2015). In this paper, we reexamine this aspect by considering whether the W-R features arise from hydrogen-rich very massive stars (VMSs; masses $> 100\,M_{\odot}$).

Crowther et al. (2010) found that four stars in R136, the central ionizing cluster of the 30 Doradus region in the Large Magellanic Cloud (LMC), have masses that exceeded the then standard upper mass limit of $150\,M_{\odot}$ (Figer 2005). The four stars they find have initial masses between 165 and $320\,M_{\odot}$, based on model fitting. More recently, Crowther et al. (2016) have presented a stellar census of the content of R136 from *HST*/STIS UV spectroscopy. They derive a cluster age of 1.5 $\pm$ 0.5 Myr and find that the He II λ1640 emission flux in the R136 cluster originates exclusively from stars with masses above $100\,M_{\odot}$.

VMSs are also expected to make a significant contribution to the ionizing flux output and account for ~25% of the ionizing photon luminosity in R136 (Doran et al. 2013). In NGC 5253, clusters #5 and #11 contribute about 40%–50% of the total ionization of the galaxy, with the majority coming from cluster #11. However, 50% of the ionizing photon rate is unaccounted for in the region of the supernebula (Calzetti et al. 2015). Turner et al. (2015) find that they need to invoke a top-heavy initial mass function (IMF) for the two nuclear clusters to provide sufficient Lyman ionizing photons given the age constraint of 4 Myr and an upper limit to the combined cluster mass (derived from the dynamical mass of the gas in the region).

Another remarkable feature of the starburst region in NGC 5253 is the presence of nitrogen-enriched (by a factor of 2–3) nebular material (Walsh & Roy 1987; Kobulnicky et al. 1997; López-Sánchez et al. 2007). Monreal-Ibero et al. (2010) have mapped the area of nitrogen enrichment and find that it peaks in the giant H II region, which contains the two nuclear star clusters, and extends up to distances of 3.″3 (50 pc). The source of the nitrogen enrichment is not clear because if it is due to the chemically enriched winds of W-R stars, then helium should also be enriched, but this has not been conclusively observed (Monreal-Ibero et al. 2013).

Instead, the idea has been put forward (Kobulnicky et al. 1997) that the N enrichment is due to the winds of late O stars, where CNO processing can produce N-rich material without the accompanying He enrichment. Since that paper, the effect of rotational mixing in O stars has shown that most fast-rotating O stars will show N enrichment at their surfaces. Recently, rotating evolutionary tracks for VMSs with LMC composition have been computed by Yusof et al. (2013) and Köhler et al. (2015). These studies find that the degree of N and He enrichment depends on rotational mixing and mass loss. In this paper, we explore whether VMSs and/or fast-rotating stars can explain the N enrichment associated with the nuclear clusters in NGC 5253.

This paper is organized as follows. In Section 2, we describe the spectroscopic observations and interpret them in Section 3. We discuss our findings that VMSs are present in cluster #5 in Section 4, and we present our summary and conclusions in Section 5.

2. OBSERVATIONS

We have obtained high spectral resolution spectroscopy across the starburst core of NGC 5253 with the UV-Visual Echelle Spectrograph (UVES) at the Very Large Telescope (VLT) in Chile (Proposal ID 73.B-0238A; L. J. Smith, P.I.). We supplement this data set with archival *HST* imaging obtained with the High Resolution Channel (HRC) of the Advanced Camera for Surveys (ACS) (Proposal ID 10609; W. Vacca, P.I.) and far-ultraviolet (FUV) spectroscopy obtained with the Space Telescope Imaging Spectrograph (STIS) and the Faint Object Spectrograph (FOS). The STIS long-slit spectrum crosses cluster #5 (Proposal ID 8232; D. Calzetti, P.I.) and has been presented in Tremonti et al. (2001) and Chandar et al. (2004). The FOS spectrum (Proposal ID 6021; H. Kobulnicky, P.I.) covers a position close to cluster #5, and the data are presented in Kobulnicky et al. (1997). All the *HST* archival data were obtained from the Mikulski Archive for Space Telescopes (MAST) and reprocessed using the standard data-reduction pipelines.

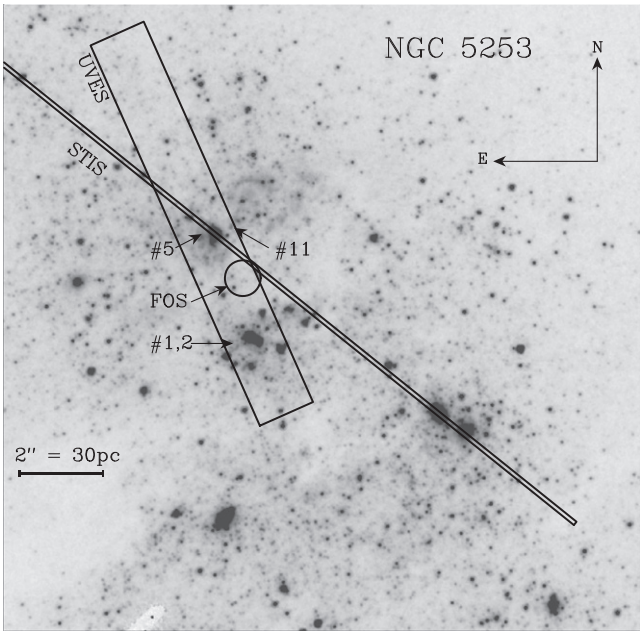

Figure 1. *HST* ACS/HRC F550M image of the central region of NGC 5253 showing the positions of the *HST*/STIS and VLT/UVES slits and the *HST*/FOS aperture. The two nuclear star clusters #5 and #11 (Calzetti et al. 2015) are indicated, as well as clusters #1, 2 corresponding to UV-1 (Meurer et al. 1995).

In Figures 1 and 2, we show the positions of the UVES, STIS, and FOS observations superimposed on ACS/HRC F550M and F658N images of the central region of NGC 5253.

2.1. STIS Spectra

Long-slit UV spectra of the nuclear region of NGC 5253 were obtained with *HST*/STIS on 1999 July 27 and comprise four exposures (totaling 10,235 s) taken with the G140L grating (1150–1730 Å) and the $52'' \times 0.''1$ slit. The slit position is shown in Figure 1 and covers 23″ on the detector. The image scale is 0.″0246 pixel^{-1} (=0.4 pc pixel^{-1}) in the spatial dimension and 0.58 Å pixel^{-1} in the spectral dimension. The spectra were co-added and extracted using a 22 pixel (=0.″54 = 8.3 pc) wide aperture for cluster #5 and the sky regions defined in Tremonti et al. (2001). The STIS spectral resolution is ≈1.8 Å or ≈360 km s^{-1} (Tremonti et al. 2001), and the spectrum was smoothed using $\sigma = 0.4$ Å, corrected for the radial velocity of this region (395 km s^{-1}; see next section)

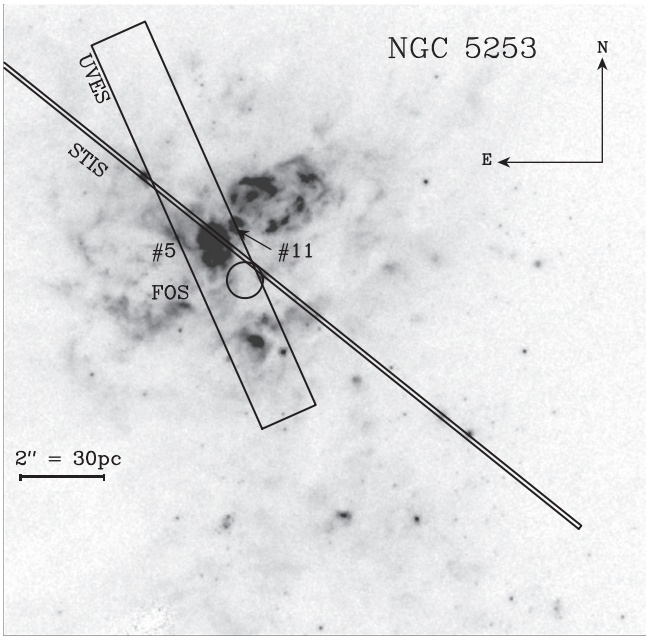

Figure 2. *HST* ACS/HRC F658N image of the central region of NGC 5253 showing the complex structure of the ionized gas and the positions of the *HST*/STIS and VLT/UVES slits, the *HST*/FOS aperture, and clusters #5 and #11.

and binned to a pixel size of 0.75 Å. The nebular O III] λλ1661, 1666 lines have measured Gaussian widths of 2.0 Å (Table 1), in agreement with the expected spectral resolution.

2.2. FOS Spectra

The FOS spectra were obtained on 1997 March 13 for a region close to cluster #5 designated HII-1 with the G190H grating (1590–2310 Å). Two exposures were taken of 2400 and 1240 s using the 0.″86 circular aperture. The spectrum is presented in Leitherer et al. (2011), and we use their observed spectrum (corrected for the radial velocity) in preference to that available from MAST because it has a better wavelength calibration. The spectral resolution is 1.4 Å for a point source and 3.2 Å for a uniform source. The nebular C III] emission line doublet has an FWHM of 3.8 Å (Table 1) or 3.1 Å, when corrected for the wavelength separation of the doublet, in good agreement with that expected for a uniform source. FOS optical spectra are also available, but the resolution and signal-to-noise ratio are too low for them to be useful compared to the ground-based optical spectra we describe in the next section.

2.3. UVES Spectra

The echelle spectra were obtained in service mode on 2004 May 4 with UVES at the VLT. At the time of observation, the red arm of UVES contained a mosaic of an EEV and an MIT-LL CCD. The blue arm had a single EEV CCD; all three CCDs have a pixel size of 15 μm. Simultaneous observations in the blue and the red were made using the standard setups with dichroic #1 (346+564 nm) and dichroic #2 (437+860 nm), covering an almost continuous wavelength region from 3100 to 10360 Å; the regions between 5610–5670 Å and 8540–8650 Å were not observed as a result of the gap between the two CCDs in the red arm.

The slit was chosen to have a position angle of 24°. As shown in Figure 1, it passes through cluster #5, and cluster #11 is on the edge of the slit. Clusters #1 and 2 (Calzetti et al. 2015) lie 2.″5 southwest of cluster #5 and correspond to the peak of the UV emission in NGC 5253 and are denoted UV-1 by Meurer et al. (1995). The slit width was 1.″4, giving a resolving power of ∼30,000 in the blue and ∼28,000 in the red.

For the observations made with dichroic #1, the target was observed at airmasses ranging from 1.5 to 1.9, with the seeing typically varying between 0.″8 and 0.″9. For dichroic #2, the range in airmass was 1.2–1.4 and the seeing was 1.″0–1.″4. In total, three exposures were taken for each waveband: two of 1425 s and one of 60 s. The third, shorter-exposure frames were taken to avoid saturating the strongest emission lines (e.g., the [O III] lines and Hα). The slit length varied between 10″ and 12″ depending on wavelength.

The observations were reduced using the Common Pipeline Library version of the ESO UVES pipeline. Spectra were extracted from the two-dimensional spectra for cluster #5 (6 pixels or 3.″3; 1 pixel = 0.″55) and also clusters #1, 2 (5 pixels or 2.″8) for comparison purposes. Sky subtraction was performed using pixels at the northern end of the slit. The full spectrum for all clusters detected and a nebular line analysis have been presented by Sidoli (2010).

3. DESCRIPTION OF THE SPECTRA

3.1. STIS and FOS UV Spectra

In Figure 3, we show the STIS and FOS UV spectra over the spectral range 1150–2000 Å. We plot them together even though they were acquired at different positions (see Figure 1) for the following reasons. There is a small overlap between the spectra in the region of the broad He II emission (see inset in Figure 3), and they both show this feature, although the profiles are slightly different, as we discuss below. To match the continuum levels, the STIS spectrum has been multiplied by a factor of 1.5. The observed F125LP filter luminosity density for cluster #5 from Calzetti et al. (2015) is plotted in Figure 3 and is in good agreement with the corrected STIS flux level.

The fact that the FOS spectrum has a strong continuum and broad He II λ1640 leads us to doubt that it represents a pure nebular spectrum offset from cluster #5. Yet, the spectrum was taken by offsetting from a star 40″ to the SW, which was acquired correctly. The position of the FOS aperture shown in Figure 1 was located using the offsets of Kobulnicky et al. (1997) and the position of the offset star on an ACS/F814W image of NGC 5253. Thus, we believe that the FOS aperture location is accurate and not centered on cluster #5. We suspect that the FOS spectrum represents reflected and/or scattered light from cluster #5 and/or cluster #11. We consider this further in Section 4. For now, we assume that the STIS and FOS spectra both represent cluster #5 and merge the two spectra in the overlap region. We note that we wish to compare UV and optical stellar emission features and the spatial extent of the UVES spectrum covers both cluster #5 and the FOS aperture location.

In Figure 4, we compare the cluster #5 UV spectrum with G140L STIS spectra of massive stars in the 1.5 Myr old LMC cluster R136 (Crowther et al. 2016, ID 12465). The stars plotted are R136a3 (WN5h; $M = 180 \pm 30\,M_{\odot}$), R136a5 (O2If/WN5; $M = 100 \pm 30\,M_{\odot}$), and R136 H36 (O2If; $M = 70 \pm 10\,M_{\odot}$), with current mass values taken from Crowther et al. (2016). These stars have been chosen because

Table 1
Emission- and Absorption-line Measurements for NGC 5253 Cluster #5

Ion	Wavelength (Å)	Line Type	Velocity (km s^{-1})	FWHM (Å)	FWHM (km s^{-1})	W_λ (Å)	10^{15} Flux (erg s^{-1} cm^{-2} Å^{-1})	Instrument
N v	1238.82, 1242.80	Stellar P Cyg em.	+730	...	...	2.2 ± 0.2	...	STIS
O v	1371.30	Stellar wind abs.	−850	...	...	1.0 ± 0.2	...	STIS
C iv	1548.20, 1550.78	Stellar P Cyg em.	+755	...	...	2.7 ± 0.3	...	STIS
		Wind terminal vel.	−2900	...	...	...	...	STIS
He ii	1640.42	Stellar em.	+460	3.8 ± 0.5	700 ± 90	3.3 ± 0.2	1.8	STIS
He ii	1640.42	Stellar em.	+140	7.0 ± 1.2	1270 ± 210	5.1 ± 0.6	3.7	FOS
He ii	1640.42	Stellar em.	+270	6.5 ± 0.6	1180 ± 100	4.2 ± 0.3	2.5	STIS+FOS
O iii]	1660.81	Neb. em.	−15	2.0 ± 0.5	370 ± 90	1.2 ± 0.1	0.7	STIS
O iii]	1666.15	Neb. em.	−40	2.0 ± 0.3	360 ± 50	1.8 ± 0.1	1.2	STIS
C iii]	1906.68, 1908.73	Neb em.	+25	3.8 ± 0.2	590 ± 30	7.7 ± 0.4	3.7	FOS
He ii	4685.71	Stellar em.	+140	22.6 ± 2.7	1450 ± 170	1.8 ± 0.1	0.380	UVES
He ii	4685.71	Neb em.	−17	2.0 ± 0.8	130 ± 50	0.17 ± 0.05	0.063	UVES

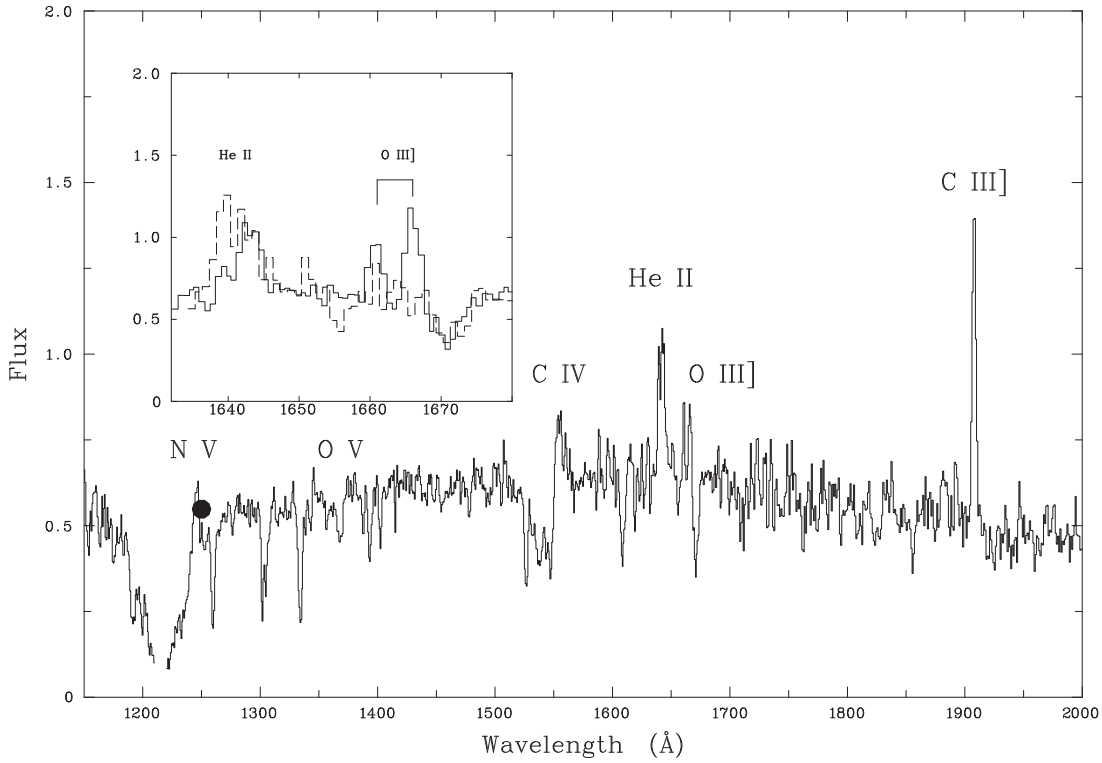

Figure 3. Merged STIS and FOS spectrum of cluster #5 over the wavelength range 1150–2000 Å. The inset plot shows the overlap region covering the He ii λ1640 emission feature for the STIS (solid line) and FOS (dashed line) spectra. The main stellar features and nebular emission lines are identified. The filled circle represents the measured luminosity density in the F125LP filter for cluster #5 from Calzetti et al. (2015). The flux is in units of 10^{-15} erg cm^{-2} s^{-1} Å^{-1}.

their spectral types bracket the spectral characteristics of the cluster #5 spectrum.

The similarity in the spectral features is striking, although the emission features are weaker in cluster #5 due to the extra continuum contribution from other cluster O stars in the spectrum. The emission- and absorption-line measurements for cluster #5 are presented in Table 1. N v λ1240, C iv λ1549, and He ii λ1640 are present in emission. O v λ1371 is detected in cluster #5 as a blueshifted absorption component with a velocity of −850 km s^{-1} (Table 1), indicating a wind-affected O v absorption. The terminal velocity measured from the C iv P Cygni absorption component is −2900 km s^{-1}, where the edge velocity has been corrected for turbulent motions in the outflow, following Crowther et al. (2016). All four spectra have weak to absent Si iv λλ1393, 1402, with interstellar absorption providing the dominant contribution. Similarly, with the exception of R136a3, they have negligible N iv] λ1486 emission.

We now discuss the He ii λ1640 emission, which is present in both the STIS and FOS spectra of cluster #5. This emission feature is resolved in both spectra, and we provide measurements in Table 1. The feature is broader and stronger in the FOS spectrum compared to the STIS spectrum (Figure 3). Beyond 1600 Å, the sensitivity of the STIS G140L grating drops by a factor of 7 and the spectrum becomes very noisy. We adopt an He ii λ1640 FWHM of 1200 km s^{-1} from the merged STIS and FOS spectra. For comparison, the FWHMs of He ii λ1640 in the R136 stars are 1490 (a3), 1040 (a5), and 1100 km s^{-1} (H36).

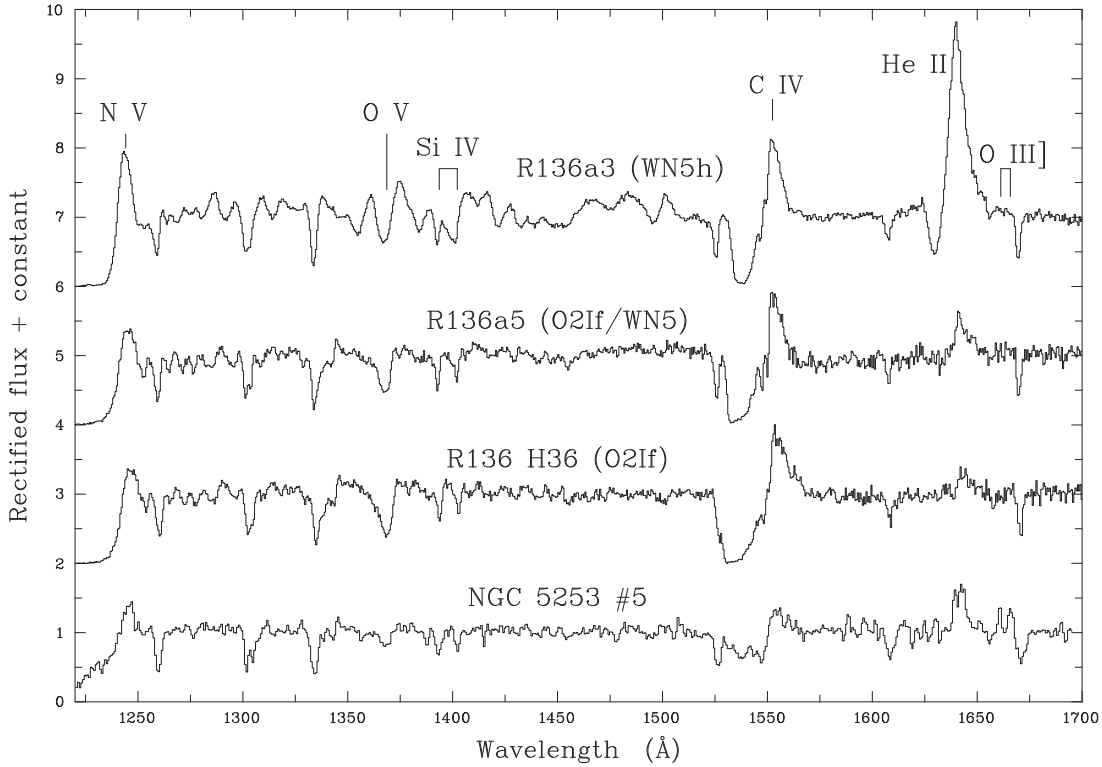

Figure 4. Rectifed *HST*/STIS+FOS spectrum of cluster #5 compared with *HST*/STIS spectra of R136a3, R136a5, and R136 H36 (Crowther et al. 2016). The main spectral features are identified.

Comparison of the relative strengths of the C IV and He II emission features in Figure 4 shows that the cluster #5 spectrum is most similar to the WN5h star R136a3 and the O2If/WN5 star R136a5. The lack of Si IV P Cygni profiles and negligible or weak N IV] λ1486 also indicates a WN5 or O2 If/WN5 spectral type (Crowther & Dessart 1998).

We now compare in Figure 5 the observed UV spectrum of cluster #5 with the integrated STIS spectrum of R136a from Crowther et al. (2016). To make this comparison, we simply scaled the R136a fluxes to the distance of NGC 5253 and tweaked the fluxes by multiplying the scaled R136a spectrum by 0.92 to match the central part of the cluster #5 spectrum. The agreement is excellent by just applying this scaling. We did not correct for the different reddenings because the color excesses of #5 and R136a are similar, with values of 0.46 (Calzetti et al. 2015) and 0.42 (Crowther et al. 2016).

The strengths, widths, and velocities of the N V, O V, and C IV lines are in excellent agreement between the two spectra. The absence of Si IV P Cygni emission is also evident in both spectra. The continuum longward of C IV is weaker in the R136a spectrum, and the He II emission FWHM at 1900 km s^{-1} is broader than the cluster #5 value of 1200 km s^{-1}. Crowther et al. (2016) classify the R136a integrated spectrum as Of/WN on the basis of an He II λ1640 equivalent width of 4.5 Å, which is below the dividing line between early O supergiants and WN5 stars at 5 Å (Crowther & Dessart 1998). The measured equivalent width for cluster #5 is 4.2 Å, also suggesting an Of/WN classification.

Crowther et al. (2016) find that 95% of the He II λ1640 emission flux in the R136a integrated spectrum originates in six stars with masses above 100 $M_{\odot}$. They suggest that the integrated spectra of young star clusters that display prominent He II λ1640 emission and O V λ1371 absorption without strong Si IV $\lambda\lambda$1393–1402 P Cygni emission are indicative of a mass function that extends beyond 100 $M_{\odot}$ and a very young age of less than 2 Myr. For cluster #5, the presence of a wind-affected O V absorption gives an upper limit to the age of 2 Myr. This implies that the He II λ1640 emission has to arise from very massive Of/WN or H-burning WN stars. The lack of prominent Si IV emission indicates that the He II λ1640 emission cannot originate in classical He-burning W-R stars with ages of 3–4 Myr.

We interpret the striking similarity between the R136a and cluster #5 spectra displayed in Figure 5 as showing that cluster #5 contains VMSs. The only other known example is the cluster NGC 3125-A1 with strong (EW = 7 Å) and broad (FWHM = 1400 km s^{-1}) He II emission and O V absorption (Chandar et al. 2004; Hadfield & Crowther 2006; Wofford et al. 2014).

3.2. UVES Optical Spectrum

The optical spectrum of cluster #5 is dominated by nebular emission lines. The only discernible stellar features are underlying Balmer absorptions to the upper Balmer nebular emission lines and broad He II λ4686 emission. The Balmer continuum is strong, signifying a very young stellar population. Calzetti et al. (2015) find that strong Balmer nebular continuum emission is present in the *HST*/WFC3 F336W images in the region of clusters #5 and #11, and that nebular line emission is present in all the other optical bands. The average velocity of the nebular emission lines is measured to be 394.6 $\pm$ 1.7 km s^{-1}, and we adopt a value of 395 km s^{-1}.

The presence of W-R stars in the optical spectra of extragalactic star-forming regions is usually inferred from the presence of broad emission bumps in the continuum near

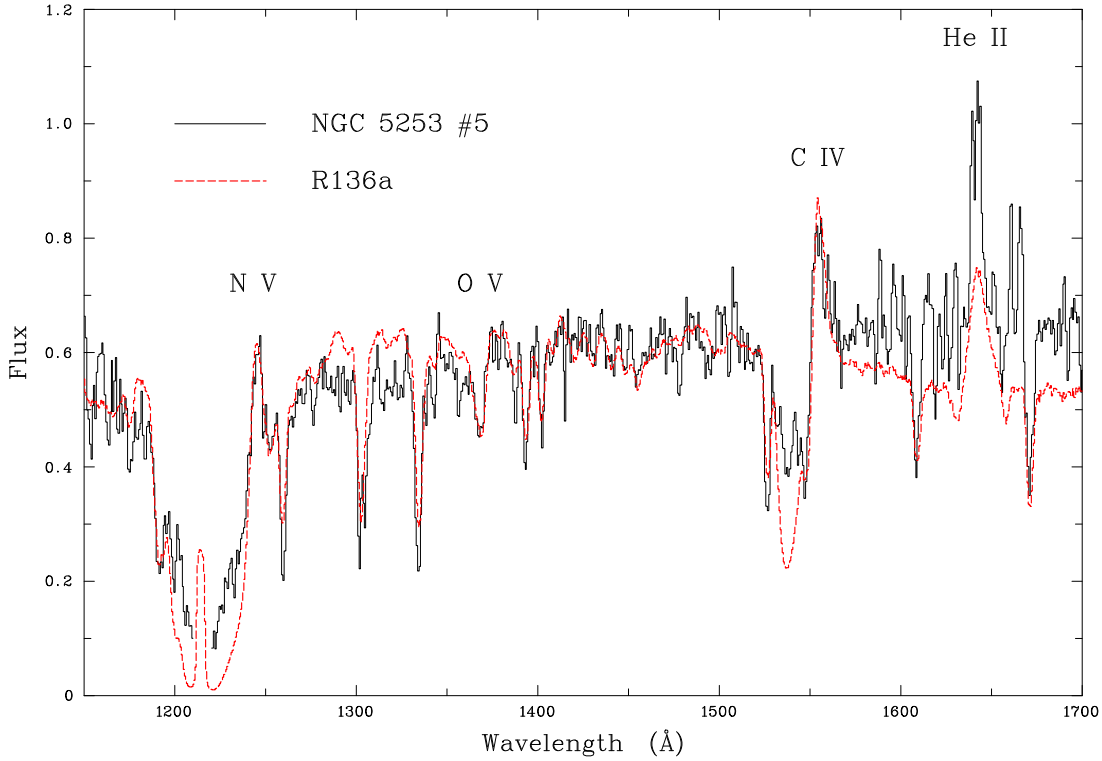

Figure 5. Integrated *HST*/STIS spectrum of R136a (Crowther et al. 2016) compared with the *HST*/STIS+FOS spectrum of cluster #5. The R136a spectrum has been scaled to the distance of NGC 5253 and multiplied by 0.92. The flux is in units of 10^{15} erg s^{-1} cm^{-2} Å^{-1}

λ4650 and λ5808. The stronger "blue bump" is due to N III $\lambda\lambda$4634–4641 and He II λ4686 emission associated with WN stars, and the weaker "red bump" is due to C IV $\lambda\lambda$5801, 5812 emission produced by WC stars. If WC stars are present, they can also contribute to the blue bump via C III λ4650. Monreal-Ibero et al. (2010) map the blue bump in the central region of NGC 5253 with integral field spectroscopy (IFS). They find WN stars associated with several clusters, including clusters #5 and #1, 2 (Figure 1). Similarly, Westmoquette et al. (2013) use IFS to map the W-R red bump. They do not detect this WC feature in cluster #5 but find that it is present in #1, 2.

In Figure 6, we show the region of the spectrum covering the W-R emission features of N III $\lambda\lambda$3634–4641, C III $\lambda\lambda$4647–4651, and He II λ4686 for clusters #5 and #1, 2. Clusters #1, 2 show the classic features of the W-R blue bump arising from both WN and WC stars, with N III, C III, and He II all present with broad emission profiles. In contrast, cluster #5 has broad He II emission only. Both spectra show the presence of nebular He II λ4686 emission. N III is present in the cluster #5 spectrum but is narrow and the individual line components are resolved. The measured average line width of the three N III lines is 1.3 Å or 81 km s^{-1} compared to the measured width of 1.2 Å or 76 km s^{-1} for nearby nebular emission lines. The N III lines are therefore likely to be nebular in origin, although detecting these transitions is unusual.

The He II λ4686 line measurements for cluster #5 are given in Table 1, corrected for nebular emission. The ratio of the nebular to stellar line flux is 17%. The UVES fluxes in Table 1 have been scaled by 0.2 to match the photometry of Calzetti et al. (2015). It should be noted that the extraction widths of the FOS (0.″86) and UVES (3.″3) apertures are very different and the fluxes of the W-R He II emission features should not be directly compared because they sample different regions.

The broad He II λ4686 emission feature in cluster #5 has an FWHM of 23 Å or 1450 km s^{-1} (cf. 1200 km s^{-1} for He II λ1640; Section 3.1). In Figure 7, we compare the cluster #5 spectrum in the region of He II λ4686 to the R136a integrated cluster spectrum, and the R136a5 and R136 H36 stellar spectra, obtained with the STIS G430M grating (S.M. Caballero-Nieves et al. 2016, in preparation). All of the spectra have similar characteristics with broad He II λ4686 emission (1910, 1130, and 1000 km s^{-1} for R136a, R136a5, and H36, respectively). The He II emission in the R136a spectrum is much stronger than that seen in cluster #5 and in other extragalactic star-forming regions with W-R stars present. This is probably because the R136a spectrum is a sum of the spectra of the most massive stars in the region and is not diluted by the continua of lower-mass stars, which will become more significant in the optical compared to the UV.

The comparison of the optical spectra of cluster #5 with R136a in the region of He II λ4686 confirms our finding from the previous section that the classification is Of/WN. We base this on the similar width of the He II feature, as well as the absence of broad N III emission. We note that the He II λ4686 emission has to be intrinsically very strong to be visible in a young massive cluster spectrum because of the continuum dilution from other stars in the slit. It is unlikely that any He II emission would be detected if only O supergiants were responsible.

4. DISCUSSION

In Section 3, we show that the spectral emission line features in the UV and optical spectra of cluster #5 can be classified as Of/WN. This is the same spectral type as the very massive young stars in R136 (Crowther et al. 2010, 2016), and the UV

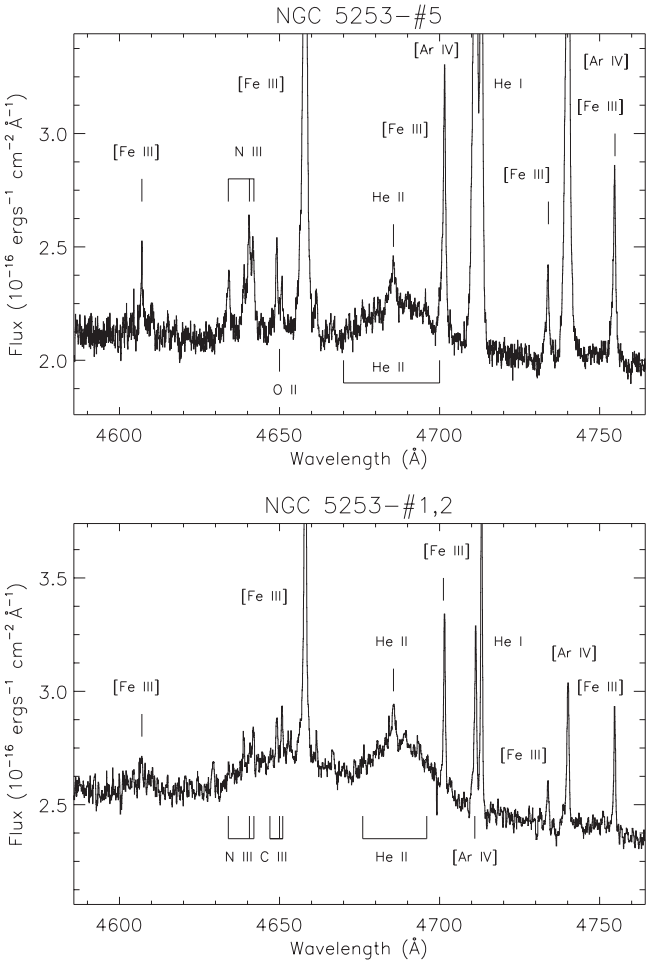

Figure 6. VLT/UVES spectrum of cluster #5 compared with clusters #1, 2. The main spectral features are identified.

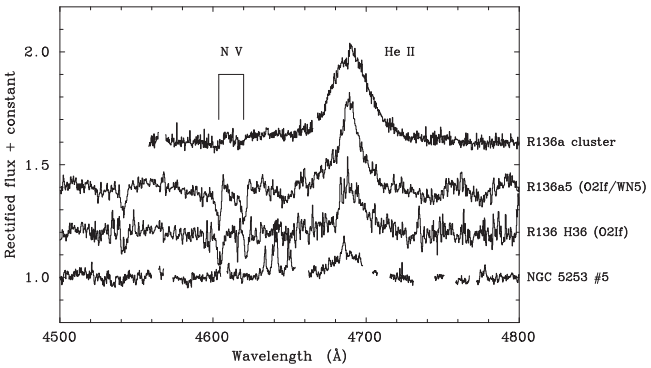

Figure 7. Rectified UVES spectrum of cluster #5 compared with *HST*/STIS spectra of R136a, R136a5, and R136 H36 (S.M. Caballero-Nieves et al. 2016, in preparation) in the region of the He II λ4686 emission feature. The nebular features in the cluster #5 spectrum have been removed.

spectra of cluster #5 and R136a are almost identical. VMSs have very dense, optically thick winds and show W-R-like broad emission lines while they are on the main sequence and hydrogen-rich. However, the presence of O V λ1371 wind absorption and the lack of UV Si IV P Cygni emission and broad optical N III emission are incompatible with classic He-burning W-R stars. As Crowther et al. (2016) discuss, the presence of O V provides an upper age limit of 2 Myr for R136. This is in accord with the very young age for cluster #5 of 1 ± 1 Myr derived by Calzetti et al. (2015) and confirmed by Wofford et al. (2016). We thus conclude that the UV and optical spectra of NGC 5253-#5 show that the cluster is 1–2 Myr old and contains stars with masses greater than 100 $M_\odot$.

In Section 3, we presented spectra for nuclear cluster #5 only. Cluster #11 has a projected separation from cluster #5 of 0.″3–0.″4 (5 pc) and is more massive and extreme in its properties (Turner et al. 2015). Calzetti et al. (2015) find that both clusters are 1 ± 1 Myr old but #11 is heavily reddened and very faint at optical wavelengths. Turner & Beck (2004) discuss whether cluster #5 is a reflection nebula generated by cluster #11. But, as discussed by Calzetti et al. (2015), the *HST* imaging shows that cluster #5 has a morphology that is consistent with a young, compact star cluster; it is slightly resolved with a size of ∼1.2 pc, symmetric, and centrally concentrated. Thus, we will assume that there are two nuclear clusters, which only differ in mass and for which all other properties are similar.

In Section 3.1, we presented FOS and STIS UV spectra, which both showed He II λ1640 broad emission, even though the FOS spectrum was obtained ∼1″ from the cluster #5 pointing for the STIS observation. The FOS spectrum clearly represents scattered light from cluster #5 and/or cluster #11. Given that the two clusters have the same age, we would also expect #11 to contain VMSs. Cluster #11 is very dusty (Calzetti et al. 2015), and thus the broad He II emission may originate from cluster #11. Given that cluster #11 is still deeply embedded in its natal gas and dust, it may be slightly younger than cluster #5, with an age of <1 Myr. Even if this was the case, it would still be expected to host a significant number of VMSs given its higher mass and the VMS main-sequence lifetime of ≈2 Myr.

4.1. Ionizing Fluxes

One of the problems with matching the observations of the NGC 5253 nuclear clusters to standard stellar population synthesis models is the lack of sufficient ionizing photons at ages of 3–5 Myr. Turner & Beck (2004) obtain a total ionizing flux $Q(\mathrm{H\,I}) = 7 \times 10^{52}\,\mathrm{s}^{-1}$, or the equivalent of 7000 O7 stars for the central 1.″2 (18 pc) from the observed 7 mm free–free continuum emission. One-third of this flux is confined to the central 5 pc region containing clusters #5 and #11. Turner et al. (2015) take the total ionizing flux, an age of 4 Myr, and the virial mass limit for this region of $1.8 \times 10^6\,M_\odot$ and compare to the predicted ionizing fluxes from Starburst99 (Leitherer et al. 1999). They find that to match the observations, a top-heavy IMF is required with a lower mass cutoff of 3 $M_\odot$.

This discrepancy can be solved if more ionizing photons are produced by the cluster stars than predicted by the stellar population synthesis models. There are potentially two ways this can be done: the inclusion of rotating massive stars (Levesque et al. 2012; Leitherer et al. 2014), and/or the inclusion of VMSs (Crowther et al. 2010; Doran et al. 2013). We consider each in turn.

Leitherer et al. (2014) present new Starburst99 models that include stellar evolutionary tracks with rotation from the Geneva group for $Z_\odot$ and $\frac{1}{7}Z_\odot$ (Ekström et al. 2012; Georgy et al. 2013). At the time, the available rotating tracks were limited, and the authors discuss the extreme case when the massive stars are rotating at 40% of their breakup velocity. Models with this level of rotation are both hotter because of the

larger helium surface abundance and more luminous because of a larger convective core. These two effects lead to a higher ionizing photon output in the Lyman continuum at ages $\geqslant$4 Myr. However, measurements of the rotational velocities of single O-type stars in the 30 Dor region show that they rotate with a rate of less than 20% of their breakup velocity (Ramírez-Agudelo et al. 2013). Thus, the ionizing outputs of the Leitherer et al. (2014) models are likely to be overestimates.

If we take the total of the derived masses for clusters #5 and #11 of $3.3 \times 10^5\,M_\odot$ and the ionizing flux of Q(H I) $= 2.2 \times 10^{52}$ s^{-1} for the central 5 pc region, Starburst99 models for a standard Kroupa IMF predict values of 1.3 (2 Myr) and 0.4 (4 Myr) $\times 10^{52}$ s^{-1} for the solar nonrotating case. For the fast-rotating models, these values rise to 1.5×10^{52} s^{-1} for both the 2 and 4 Myr cases. The metallicity of NGC 5253 is 35% solar (Monreal-Ibero et al. 2010), and Q(H I) will increase compared to solar because of the lower wind opacities. Indeed, the nonrotating SMC metallicity tracks with Starburst99 predict values of Q(H I) of 1.6 and 0.6×10^{52} s^{-1} for 2 and 4 Myr, respectively. All of these values fall short of the required ionizing flux by 30%–80%.

If massive O stars rotate as fast as 40% of their breakup velocity at SMC metallicity, the predicted values of Q(H I) may increase sufficiently to agree with the observed ionizing flux. But this is unlikely to work because the comparisons above assume the cluster masses derived from the nonrotating Starburst99 models, which fit the observed cluster SEDs from the UV to the IR (Calzetti et al. 2015). As Leitherer et al. (2014) discuss, the higher luminosities of fast-rotating massive stars will lead to bluer SEDs and lower star cluster masses as the theoretical L/M is higher. Thus, it is unlikely that rotating massive stars can provide the deficit of ionizing photons in the nuclear clusters of NGC 5253.

Doran et al. (2013) provide a census of the hot luminous stars in R136 and the 30 Dor region of the LMC. The R136 cluster (<5 pc) has a mass of $5.5 \times 10^4\,M_\odot$ (Hunter et al. 1995) and an age of 1.5 ± 0.5 Myr (Crowther et al. 2016). It contains nine VMSs (Crowther et al. 2016) inside the half-light radius of 1.7 pc (Hunter et al. 1995). Doran et al. (2013) find Q(H I) $= 7.5 \times 10^{51}$ s^{-1} for the R136 region. They compare this output to nonrotating Starburst99 models and find that the predicted ionizing flux is a factor of two lower than their empirical value at 2 Myr. The upper mass in the Starburst99 models is $100\,M_\odot$, and thus the contributions from stars with masses higher than this are ignored. Doran et al. (2013) have eight such stars located in the R136 region, and by excluding these stars, they find much better agreement with the Starburst99 models. The four WN5h stars in R136 have a combined ionizing flux of Q(H I) $= 2 \times 10^{51}$ s^{-1} and are responsible for 25% of the ionizing flux. For the two NGC 5253 nuclear clusters, if we take the predicted ionizing flux from Turner & Beck (2004) of Q(H I) $= 2.2 \times 10^{52}$ s^{-1} and the predicted ionizing flux from Starburst99 of Q(H I) $= 1.6 \times 10^{52}$ s^{-1} for SMC metallicity and nonrotating tracks at 2 Myr, then the deficit amounts to 6×10^{51} s^{-1}, or the equivalent of 12 WN5h stars with masses $\geqslant 150\,M_\odot$. Given the six times greater mass for clusters #5 and #11 compared to R136, this number seems reasonable. The addition of VMSs will hardly change the cluster SED because of their small numbers. These types of stars are not expected to have an appreciable flux below the He II Lyman limit because of their dense winds. Their presence cannot therefore explain the He II λ4686 nebular emission (Section 3.2).

4.2. Origin of the Nitrogen Enrichment

Monreal-Ibero et al. (2010, 2012) use IFS to map out the nebular N enrichment. They find that it peaks ($\approx$3 times overabundant) at the position of the two nuclear clusters and covers an area 65 × 30 pc corresponding to the giant H II region associated with the clusters (Figure 2). The source of this enrichment is unexplained because the He abundance should also be enhanced if the pollution is caused by the chemically enriched winds of W-R stars, but this has not been seen with any certainty (Monreal-Ibero et al. 2013).

Köhler et al. (2015) present an evolutionary model grid at LMC metallicity for stars in the H-burning phase with initial masses from 70 to $500\,M_\odot$ and rotational velocities from 0 to 550 km s^{-1}. They find that N enrichment is ubiquitous because rotational mixing and/or mass loss quickly leads to the establishment of CNO equilibrium abundances in the atmospheric layers. Whether surface He enrichment occurs is more complicated and depends on the mass of the star through the mass-loss rate and the rotation velocity.

As an illustrative example, the Köhler et al. (2015) evolutionary track for a $100\,M_\odot$ star rotating at 200 km s^{-1} (20% of the critical velocity) reaches CNO equilibrium surface abundances at an age of 1 Myr, and the surface N abundance equals the enriched value observed in NGC 5253 at an age of only 0.26 Myr. In this model, the He abundance does not start to increase until an age of 2.2 Myr. At an age of 1 Myr, the star has lost $4.5\,M_\odot$ of its original mass. We now consider whether such massive, rotating O stars can produce the observed level of N enrichment over a timescale of ~1 Myr.

Observationally, the nebular emission line components are composed of three components with the N-enriched material confined to a broad component with an FWHM of 100–150 km s^{-1}, an electron density of 500 cm^{-3}, and a linear velocity gradient from -50 to $+50$ km s^{-1} over the central 4″ centered on cluster #5 (Monreal-Ibero et al. 2010; Sidoli 2010; Westmoquette et al. 2013). Taking the outflow velocity as 70 km s^{-1} and a size of 65 pc for the N-enriched region (Monreal-Ibero et al. 2012; Westmoquette et al. 2013), we find a dynamical timescale for the pollution of 0.5 Myr. Thus, there is sufficient time for clusters #5 and #11 to have polluted their environment despite their young age of 1–2 Myr.

We can derive the mass of the excess N by assuming that the region is cylindrical with a radius of 15 pc and an enriched log N/O $= -0.81$ compared to -1.37 in unenriched knot #2 (Monreal-Ibero et al. 2012). The resulting mass of excess N is 1–10 $M_\odot$, assuming a volume filling factor of 0.01–0.1 for the ionized gas. If we assume an average stellar surface N enrichment of a factor of 10 (Köhler et al. 2015), giving a nitrogen mass fraction of 7.6×10^{-4}, then the stellar mass-loss rate required to deposit $1\,M_\odot$ of N in 1 Myr is $1.3 \times 10^{-3}\,M_\odot$ yr^{-1}. For a Kroupa (2001) IMF extending to $300\,M_\odot$, there should be 300 stars more massive than $50\,M_\odot$ for the combined cluster mass of $3.3 \times 10^5\,M_\odot$, giving a reasonable average stellar mass-loss rate of $4.4 \times 10^{-6}\,M_\odot$ yr^{-1}. While these calculations are approximate, they demonstrate that the observed N enrichment associated with clusters #5 and #11 can be produced by the stellar winds of massive ($>50\,M_\odot$), rotating cluster O stars in the first million years. The presence of VMSs in the two clusters will increase the

amount of enriched nitrogen produced because they rapidly (<0.5 Myr) reach CNO equilibrium abundances on their surfaces and have very high mass-loss rates ($>10^{-5}\,M_{\odot}\,\mathrm{yr}^{-1}$), particularly if they are close to their Eddington limits.

At an age of 1 Myr, the lower-mass stars in the NGC 5253 nuclear clusters will still be forming and thus may be nitrogen enriched. This is of relevance to models seeking to explain multiple stellar generations in globular clusters using fast-rotating massive stars as the source of self-enrichment (Decressin et al. 2007).

4.3. Comparison with He II-emitting High-redshift Galaxies

The UV spectrum of cluster #5 is representative of a very young, nearby, low-metallicity, nuclear starburst. It bears a striking resemblance to the UV rest-frame spectrum of Q2343-BX418 (Erb et al. 2010). These authors suggest that this $z = 2.3$ young, low-mass, low-metallicity galaxy is a plausible analog to the young, low-metallicity star-forming galaxies at $z > 5$. Q2343-BX418 has broad He II λ1640 emission ($1000\,\mathrm{km\,s}^{-1}$) with a rest equivalent width of 2.7 Å, and nebular emission from O III] $\lambda\lambda$1661, 1666 and C III] $\lambda\lambda$1907, 1909 is also detected. The C III] equivalent width of 7.1 Å is very similar to the value of 7.7 Å that we measure for the FOS spectrum near cluster #5. Rigby et al. (2015) discuss measurements of C III] emission in nearby and high-redshift galaxies. In their nearby sample, they include the FOS spectrum of NGC 5253 used here and note that this galaxy is one of the 20% of local galaxies that show strong C III] emission.

Cassata et al. (2013) identified 39 He II λ1640 emitting galaxies over a redshift range of 2–4.6 from deep survey data. They classify the He II emitters into two different classes depending on the width of the emission. They explain the broad emission (FWHM $> 1200\,\mathrm{km\,s}^{-1}$) with W-R stars and suggest that for the 11 objects with unresolved He II λ1640 emission (FWHM $< 1200\,\mathrm{km\,s}^{-1}$), the emission is nebular in origin and powered by either the strong ionizing radiation field from a stellar population that is rare at $z \sim 0$ or Population III star formation.

Gräfener & Vink (2015) discuss the possibility that the narrow He II emission arises from a population of VMSs at low metallicity and show that the predicted He II line strengths and widths are in line with those expected for a population of VMSs in young super star clusters located in the galaxies of the Cassata et al. (2013) sample. We note that we measure an He II λ1640 line width of $1200\,\mathrm{km\,s}^{-1}$ for cluster #5, which is at the borderline between the two groups of He II emitters identified by Cassata et al. (2013). Moreover, we identify this emission as originating in VMSs.

The presence of VMSs in young, high-redshift galaxies has important consequences for the ionizing photon budget and cosmic reionization. As Doran et al. (2013) and this paper (Section 4.1) have shown, VMSs increase the number of ionizing photons by up to a factor of two for the first 1–3 Myr of a starburst compared to standard spectral synthesis models, which typically have upper mass cutoffs of $100\,M_{\odot}$. Interestingly, Zastrow et al. (2013) find evidence for the escape of ionizing photons in two out of seven nearby dwarf starbursts through the detection of ionization cones. These two galaxies are NGC 5253 and NGC 3125, the latter of which also has a UV spectrum indicative of VMSs (Wofford et al. 2014).

The *James Webb Space Telescope* (*JWST*) will obtain rest-frame UV spectra of high-redshift star-forming galaxies. These spectra may reveal the presence of VMSs through the presence of He II emission and O V wind absorption and the absence of Si IV P Cygni emission. It is crucial to extend the current suite of stellar population synthesis models to cutoff masses greater than $100\,M_{\odot}$ in order to model their properties correctly.

5. SUMMARY AND CONCLUSIONS

We have examined UV and optical spectroscopy of cluster #5 in the nucleus of NGC 5253 with the aim of reconciling the extremely young age of 1 ± 1 Myr found by Calzetti et al. (2015) with the presence of W-R features in the cluster spectrum. Specifically, we have investigated whether the W-R features arise from hydrogen-rich VMSs with masses greater than $100\,M_{\odot}$. In addition, the presence of VMSs may be necessary to account for the 50% deficit in the ionizing photon rate (Calzetti et al. 2015) and the nitrogen-enriched nebular gas.

We present archival STIS and FOS UV spectra of cluster #5 and compare them with STIS spectra of VMSs in R136, the central ionizing cluster of 30 Dor in the LMC, and the R136a integrated spectrum from Crowther et al. (2016). We detect broad ($1200\,\mathrm{km\,s}^{-1}$) He II λ1640 emission, O V λ1371 wind absorption, C IV P Cygni emission, and an absence of Si IV P Cygni emission. These spectral characteristics are only compatible with a very young age (<2 Myr) and a mass function that extends beyond $100\,M_{\odot}$. The UV spectrum of #5 is extremely similar to the integrated spectrum of the R136a cluster, which contains six VMSs (Crowther et al. 2016).

We compare the cluster #5 VLT/UVES spectrum in the region of He II λ4686 to another cluster in NGC 5253, containing classical W-R stars, the individual VMSs in R136, and the R136a cluster. We find that cluster #5 has broad He II emission and an absence of other broad features due to N III or C III, which are usually seen in clusters containing W-R stars. Again, the spectrum is most similar to the R136a spectrum and confirms our finding from the UV spectrum that VMSs are present in cluster #5.

We conclude from the UV and optical comparisons that NGC 5253-5 is very young, with an age of less than 2 Myr, and that the broad He II emission is produced by VMSs that have dense, optically thick winds and show W-R-like emission features while they are on the main sequence.

We consider whether the 50% discrepancy in the predicted and observed ionizing flux for the nuclear region of NGC 5253 can be solved by increasing the number of ionizing photons produced by the cluster stars. We compared Q(H I) to the output of Starburst99 models that include fast-rotating massive star evolutionary tracks (Leitherer et al. 2014). We find that these models are unlikely to work because they do not produce sufficient ionizing photons and alter the cluster SED, which is well fitted by nonrotating Starburst99 models (Calzetti et al. 2015). We consider whether VMSs can account for the photon deficit by using the empirical results of Doran et al. (2013) for R136. They find that the four WN5h stars account for 25% of the R136 ionizing flux. At an age of 2 Myr, the predicted ionizing flux from Starburst99 (Leitherer et al. 1999) at SMC metallicity is 30% less than the observed ionizing flux within the central 5 pc. The equivalent of 12 WN5h stars with masses $>150\,M_{\odot}$ is required to make up the deficit, which is reasonable given that the combined cluster mass of #5 and #11 is six times more massive than R136.

We investigated the origin of the nitrogen enrichment in the giant H II region surrounding the nuclear clusters. The dynamical timescale for the enrichment is 0.5 Myr, well within the age of 1–2 Myr for the nuclear clusters. We find that the mass of enriched nitrogen is 1–10 $M_{\odot}$ depending on the filling factor of the ionized gas. Rapid surface nitrogen enrichment occurs through mass loss and/or rotational mixing in the new evolutionary model grid of Köhler et al. (2015), which includes stars up to 500 $M_{\odot}$ with rotation for LMC composition. We find that the mass of excess N can be produced by rotating massive stars in the clusters if surface CNO equilibrium abundances are achieved within the first 1 Myr, as indicated by the Köhler et al. (2015) models. We note that the lower-mass stars, which are presumably still forming, may be nitrogen rich. The nuclear region of NGC 5253 is probably observationally unique in containing very young star clusters, which have already polluted their environments with the chemically enriched winds of massive stars.

We compare the UV spectrum of cluster #5 with those of metal-poor, high-redshift galaxies and show that it has many similarities in terms of the He II emission line strength and width and the presence of strong O III] $\lambda\lambda$1661, 1666 and C III] $\lambda\lambda$1907, 1909 nebular emission. VMSs may exist in young star-forming regions at high redshift, and their presence should be revealed by UV rest-frame spectra to be obtained by *JWST*. Population synthesis models typically have upper mass cutoffs of 100 $M_{\odot}$. It is crucial to extend these into the VMS regime to correctly account for the radiative, mechanical, and chemical feedback, which will be dominated by VMSs for the first 1–3 Myr in star-forming regions.

We thank Ed Churchwell, Jay Gallagher, Selma de Mink, Hugues Sana, Christy Tremonti, and Aida Wofford for enlightening discussions. Based on observations collected at the European Organisation for Astronomical Research in the Southern Hemisphere under ESO program 73.B-0238(A). Based on observations made with the NASA/ESA *Hubble Space Telescope*, obtained from the Mikulski Archive for Space Telescopes (MAST) at the Space Telescope Science Institute, which is operated by the Association of Universities for Research in Astronomy, Inc., under NASA contract NAS5-26555.

Facilities: HST (STIS, FOS, ACS/HRC), VLT: Kueyen (UVES).

REFERENCES

Alonso-Herrero, A., Takagi, T., Baker, A. J., et al. 2004, ApJ, 612, 222
Asplund, M., Grevesse, N., Sauval, A. J., & Scott, P. 2009, ARA&A, 47, 481
Beck, S. C., Turner, J. L., Ho, P. T. P., Lacy, J. H., & Kelly, D. M. 1996, ApJ, 457, 610
Caldwell, N., & Phillips, M. M. 1989, ApJ, 338, 789
Calzetti, D., Johnson, K. E., Adamo, A., et al. 2015, ApJ, 811, 75
Calzetti, D., Meurer, G. R., Bohlin, R. C., et al. 1997, AJ, 114, 1834
Campbell, A., Terlevich, R., & Melnick, J. 1986, MNRAS, 223, 811
Cassata, P., Le Fèvre, O., Charlot, S., et al. 2013, A&A, 556, A68
Chandar, R., Leitherer, C., & Tremonti, C. A. 2004, ApJ, 604, 153
Crowther, P. A., Beck, S. C., Willis, A. J., et al. 1999, MNRAS, 304, 654
Crowther, P. A., Caballero-Nieves, S. M., Bostroem, K. A., et al. 2016, MNRAS, 458, 624
Crowther, P. A., & Dessart, L. 1998, MNRAS, 296, 622
Crowther, P. A., Schnurr, O., Hirschi, R., et al. 2010, MNRAS, 408, 731
Davidge, T. J. 2007, AJ, 134, 1799
Decressin, T., Charbonnel, C., & Meynet, G. 2007, A&A, 475, 859
Doran, E. I., Crowther, P. A., de Koter, A., et al. 2013, A&A, 558, A134
Ekström, S., Georgy, C., Eggenberger, P., et al. 2012, A&A, 537, A146
Erb, D. K., Pettini, M., Shapley, A. E., et al. 2010, ApJ, 719, 1168
Figer, D. F. 2005, Natur, 434, 192
Freedman, W. L., Madore, B. F., Gibson, B. K., et al. 2001, ApJ, 553, 47
Georgy, C., Ekström, S., Eggenberger, P., et al. 2013, A&A, 558, A103
Gräfener, G., & Vink, J. S. 2015, A&A, 578, L2
Hadfield, L. J., & Crowther, P. A. 2006, MNRAS, 368, 1822
Hunter, D. A., Shaya, E. J., Holtzman, J. A., et al. 1995, ApJ, 448, 179
Karachentsev, I. D., Tully, R. B., Dolphin, A., et al. 2007, AJ, 133, 504
Kobulnicky, H. A., Skillman, E. D., Roy, J.-R., Walsh, J. R., & Rosa, M. R. 1997, ApJ, 477, 679
Köhler, K., Langer, N., de Koter, A., et al. 2015, A&A, 573, A71
Kroupa, P. 2001, MNRAS, 322, 231
Leitherer, C., Ekström, S., Meynet, G., et al. 2014, ApJS, 212, 14
Leitherer, C., Schaerer, D., Goldader, J. D., et al. 1999, ApJS, 123, 3
Leitherer, C., Tremonti, C. A., Heckman, T. M., & Calzetti, D. 2011, AJ, 141, 37
Levesque, E. M., Leitherer, C., Ekstrom, S., Meynet, G., & Schaerer, D. 2012, ApJ, 751, 67
López-Sánchez, Á R., Esteban, C., García-Rojas, J., Peimbert, M., & Rodríguez, M. 2007, ApJ, 656, 168
López-Sánchez, Á R., Koribalski, B. S., van Eymeren, J., et al. 2012, MNRAS, 419, 1051
Meurer, G. R., Heckman, T. M., Leitherer, C., et al. 1995, AJ, 110, 2665
Monreal-Ibero, A., Vílchez, J. M., Walsh, J. R., & Muñoz-Tuñón, C. 2010, A&A, 517, A27
Monreal-Ibero, A., Walsh, J. R., & Vílchez, J. M. 2012, A&A, 544, A60
Monreal-Ibero, A., Walsh, J. R., Westmoquette, M. S., & Vílchez, J. M. 2013, A&A, 553, A57
Ramírez-Agudelo, O. H., Simón-Díaz, S., Sana, H., et al. 2013, A&A, 560, A29
Rigby, J. R., Bayliss, M. B., Gladders, M. D., et al. 2015, ApJL, 814, L6
Schaerer, D., Contini, T., Kunth, D., & Meynet, G. 1997, ApJL, 481, L75
Sidoli, F. 2010, PhD thesis, University of London
Tremonti, C. A., Calzetti, D., Leitherer, C., & Heckman, T. M. 2001, ApJ, 555, 322
Tully, R. B., Courtois, H. M., Dolphin, A. E., et al. 2013, AJ, 146, 86
Tully, R. B., Libeskind, N. I., Karachentsev, I. D., et al. 2015, ApJL, 802, L25
Turner, J. L., & Beck, S. C. 2004, ApJL, 602, L85
Turner, J. L., Beck, S. C., Benford, D. J., et al. 2015, Natur, 519, 331
Turner, J. L., Beck, S. C., & Ho, P. T. P. 2000, ApJL, 532, L109
Turner, J. L., Ho, P. T. P., & Beck, S. C. 1998, AJ, 116, 1212
van den Bergh, S. 1980, PASP, 92, 409
Walsh, J. R., & Roy, J.-R. 1987, ApJL, 319, L57
Westmoquette, M. S., James, B., Monreal-Ibero, A., & Walsh, J. R. 2013, A&A, 550, A88
Wofford, A., Charlot, S., Bruzual, G., et al. 2016, MNRAS, 457, 4296
Wofford, A., Leitherer, C., Chandar, R., & Bouret, J.-C. 2014, ApJ, 781, 122
Yusof, N., Hirschi, R., Meynet, G., et al. 2013, MNRAS, 433, 1114
Zastrow, J., Oey, M. S., Veilleux, S., & McDonald, M. 2013, ApJ, 779, 76